All-Weather Automotive Perception: Monte Carlo Simulation of FMCW LiDAR-Radar Sensor Fusion in Foggy Conditions

Yassine El haddioui[1,1,*], *Zhour* Madini[2,1], *Nour* Alem[3,2], and *Younes* Zouine[4,1]

[1]Department Electrical and Telecommunication, Laboratory of Advanced Systems Engineering (ISA), National School of Applied Sciences (ENSA), Ibn Tofail University, Kenitra,14000, Morocco
[2]Institute of Applied Physics, Mohammed 6 Polytechnic University, Benguerir, MOROCCO

Abstract. This work presents an end-to-end Monte Carlo-based framework for FMCW LiDAR-radar fusion in fog, targeting all-weather automotive perception. The model couples radiative-transfer simulation of FMCW LiDAR with a 77 GHz radar link-budget formulation, jointly capturing optical scattering, attenuation, and RF propagation within the same fog microphysical environment. Through integrated beat-spectrum and range Doppler synthesis, the framework quantifies visibility-dependent degradation, clutter evolution, and cross-sensor complementarity. An adaptive fusion kernel balances LiDAR spatial precision with radar penetration as visibility decreases. Simulations over visibilities of 0.1–2.0 km show that while LiDAR alone fails beyond ~70 m in dense fog, the fused system sustains >100 m detection at $P_d = 0.9$, $P_{fa} = 10^{-3}$. By linking Monte Carlo radiative physics with probabilistic sensor fusion, this study delivers the first quantitative analysis of FMCW LiDAR–radar synergy under scattering-limited conditions, advancing the foundation of all-weather autonomous perception.

1 Introduction

The deployment of autonomous vehicles (AVs) underpins the vision of sustainable and intelligent mobility. However, the reliability of perception sensors in adverse weather remains a major barrier to widespread adoption. Among available modalities, LiDAR is central to environment mapping due to its centimeter-scale resolution and ability to generate dense 3D point clouds [1]. Yet, its performance deteriorates sharply in fog, where Mie scattering by micron-scale droplets induces volumetric backscatter, range loss, and signal-to-noise degradation [2]. Conversely, millimeter-wave (mmWave) radar remains largely unaffected by these scattering effects, providing stable range and velocity measurements in dense fog, rain, and snow [3]. However, radar's lower spatial fidelity limits its use for detailed scene reconstruction and object classification. The complementarity of these two modalities LiDAR for spatial precision and radar for penetration robustness has motivated extensive industrial and academic work in multi-sensor fusion for advanced driver-assistance systems (ADAS) and autonomous driving [4]. Nonetheless, most existing studies treat each modality in isolation. LiDAR-focused

*e-mail: yassine.elhaddioui@uit.ac.ma

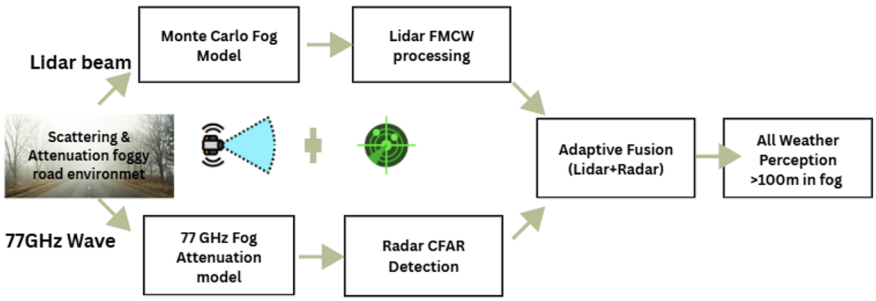

Figure 1. Conceptual framework of LiDAR–Radar sensor fusion for robust perception in foggy conditions. LiDAR provides high-resolution spatial information but degrades in fog due to scattering, while radar maintains stable long-range detection.

analyses often rely on empirical attenuation models or simplified photon-transport simulations that neglect FMCW signal synthesis [5], while radar studies rarely account for joint modeling with optical sensors or wavelength-specific fog microphysics. Furthermore, few investigations perform systematic visibility sweeps across realistic fog conditions (0.1–2.0 km), which are essential to characterize the transition between optical and RF dominance. To address these gaps, this paper develops a Monte Carlo-based physics-driven framework that unifies FMCW LiDAR radiative-transfer modeling with a 77 GHz radar propagation model under shared fog microphysical conditions [6]. The framework jointly simulates photon scattering, signal synthesis, and range-Doppler formation to produce consistent LiDAR and radar degradation metrics. Through this unified approach, we:

1. Quantitatively couple wavelength-dependent scattering and extinction phenomena with FMCW LiDAR signal formation, establishing a direct link between fog microphysics and sensor-level SNR and clutter dynamics.

2. Demonstrate the efficacy of LiDAR–Radar fusion under varying visibilities (0.1–2.0 km), showing how adaptive probabilistic weighting preserves detection continuity from dense fog to light haze.

3. Deliver a validated, Monte Carlo–driven simulation framework that unifies optical radiative transfer and radar propagation models, enabling the design of energy-efficient, all-weather automotive perception systems without reliance on extensive field testing.

2 Literature review

The challenge of reliable sensing in adverse weather has been studied for decades, beginning with radar as one of the earliest candidates for robust navigation. H. Su et al [7] demonstrated that probabilistic radar-based SLAM could operate in environments where optical sensors struggled, though the limited angular resolution and clutter susceptibility of radar reduced its suitability for fine-grained mapping. This gap encouraged the rise of LiDAR, which offers centimeter-scale resolution and dense 3D point clouds. However, from the outset LiDAR's vulnerability to fog and smoke was noted, as atmospheric scattering and absorption truncate the detection range and introduce false returns. By the mid-2010s, researchers began quantifying this degradation systematically.

Table 1. Summary of related work on LiDAR and Radar sensing in adverse weather

Year	Study	Sensors	Key Findings	Limitation (Gap)
2023	C. Yuen [14]	Radar	Radar-SLAM feasible in poor visibility	Poor angular resolution; limited mapping fidelity
2016	Fritsche et al. [15]	LiDAR + Radar	MPR concept; radar substitutes fog-corrupted LiDAR points	Fusion heuristic only; no FMCW or wavelength analysis
2017	Jie Hu, Lei Wang [16]	LiDAR + Radar + Thermal	Hazard detection robust in smoke	Task-specific; not automotive-scale
2022	Jiaxin Li, Danfeng Hong [17]	LiDAR + Camera + Radar	Dataset + deep multimodal fusion; robust detection without fog labels	Data-driven; no physics modeling
2021	W. Oing, Z. Bin and C. [18]	Full-Waveform LiDAR	Waveform processing recovers hidden returns	Complexity and cost; no radar integration
2024	Yang et al. [19]	LiDAR + Radar	RaLiBEV BEV fusion; strong robustness in fog	Perception-level only; no Monte Carlo or wavelength physics
2025	This work	FMCW LiDAR (905/1310/1550 nm) + Radar	Monte Carlo + FMCW beat synthesis + radar fusion; SNR, CNR, ROC across visibilities	First physics-grounded study of wavelength trade-offs + fusion

Fritsche et al. [8] introduced the Mechanically Pivoting Radar (MPR) concept to complement LiDAR in fog chamber experiments. Their results showed that radar points could substitute corrupted LiDAR measurements, enabling mapping and SLAM in foggy environments. The automotive community formalized these insights with controlled fog-chamber ben0chmarks. hazar chabani et al. [9] reported that under meteorological visibility below 40 m, commercial 905 nm LiDARs lost most detection capability beyond 25 m, even with parameter tuning. Their later work, "Seeing Through Fog" [10], provided one of the first large-scale multimodal datasets (LiDAR–camera–radar) in natural fog and showed that fusion with uncertainty-aware deep learning improves detection robustness without explicit fog labels. Other researchers explored waveform-level processing. Tan Zhou, et al. [11] argued that full-waveform LiDAR (FWL) could recover more returns under obscurants than discrete-return processing, moving LiDAR closer to radar's penetrative robustness. Tent experiments confirmed the potential, but challenges in computational load and detector cost limited practical adoption. The latest wave of research leverages learning-based radar-LiDAR fusion.

Yang et al. [12] introduced RaLiBEV, an anchor-free Bird's-Eye-View (BEV) fusion detector with an interactive transformer backbone. Validated on the Oxford Radar RobotCar dataset, RaLiBEV improved detection in foggy scenarios by up to 19% compared to earlier fusion networks, confirming radar's complementary value when LiDAR point density collapses. However, critical gaps remain. Few studies explicitly model the wavelength dependence of LiDAR in fog (905 vs. 1310 vs. 1550 nm), despite Mie scattering theory predicting large performance differences. Similarly, while radar fusion is now standard at the perception level, no prior work has unified Monte Carlo radiative-transfer simulation of FMCW LiDAR with radar propagation modeling to generate physics-grounded fusion metrics such as SNR, clutter-to-noise ratio (CNR), and ROC curves across visibility regimes [13].

Our work addresses this gap by introducing a Monte Carlo-based simulator for FMCW LiDAR at 905, 1310, and 1550 nm under fog, coupled with an analytical mmWave radar model. By synthesizing beat spectra and fusion ROC curves, we provide the first physics-driven evaluation of LiDAR-Radar fusion for all-weather automotive perception.

3 Methodology

The proposed framework combines Monte Carlo radiative transfer for FMCW LiDAR, a 77-GHz radar link budget with fog attenuation, and a visibility-adaptive fusion policy. This section details the mathematical models and technical assumptions that underpin the simulation.

3.1 FMCW LiDAR Channel Under Fog

a) Fog microphysics

Fog droplets are modeled using a log-normal size distribution [20]:

$$n(r) = \frac{N_0}{r\,\sigma_g\,\sqrt{2\pi}} \exp\left[-\frac{(\ln r - \ln r_m)^2}{2\sigma_g^2}\right], \tag{1}$$

where r_m and σ_g denote the modal radius and geometric spread. Two modeling modes are implemented:

- **Empirical visibility mode:** The bulk extinction coefficient is derived from meteorological visibility V via Koschmieder's law,

$$\beta_{\text{ext}} = \frac{3.912}{V}, \qquad [\text{m}^{-1}], \tag{2}$$

  with single-scattering albedo $\omega_0 \in [0.7, 0.95]$ and anisotropy $g \in [0.75, 0.9]$ typical of advection fog.

- **Physics-based mode:** Mie theory computes Q_{ext}, Q_{sca}, and g, integrated over $n(r)$ to yield wavelength-dependent properties $\beta_{\text{ext}}(\lambda), \omega_0(\lambda), g(\lambda)$.

c) Radiative-transfer Monte Carlo

Photon packets are propagated with Gaussian divergence, sampling free paths as

$$s = -\frac{\ln \xi}{\beta_{\text{ext}}}, \qquad \xi \sim \mathcal{U}(0, 1). \tag{3}$$

At each event, photons scatter with probability ω_0 or are absorbed otherwise. Scattering angles follow the Henyey–Greenstein phase function [20]:

$$p(\cos\theta \mid g) = \frac{1 - g^2}{4\pi(1 + g^2 - 2g\cos\theta)^{3/2}}. \tag{4}$$

Packets within the receiver FOV contribute to the depth-resolved backscatter histogram $B(t; \lambda)$, while two-way transmittance is approximated as

$$T^2(R; \lambda) = \exp[-2\beta_{\text{ext}}(\lambda)R]. \tag{5}$$

Energy conservation is verified numerically, with total deviations $< 0.5\%$ across runs.

d) FMCW baseband synthesis

For a linear chirp of bandwidth B_c and duration T_c, slope $S = B_c/T_c$, a target at range R produces beat frequency

$$f_b = \frac{2SR}{c}, \qquad \tau = \frac{2R}{c}. \tag{6}$$

Range resolution and unambiguous range are

$$\Delta R = \frac{c}{2B_c}, \qquad R_{\max} = \frac{cF_s}{2S}, \tag{7}$$

with sampling rate F_s. The heterodyne photocurrent is

$$i(t) = 2R_d \sqrt{P_{\mathrm{LO}} P_{\mathrm{sig}}} \cos(2\pi f_b t + \phi), \tag{8}$$

where R_d is detector responsivity. Noise sources include shot, thermal, and digitization noise. The LiDAR SNR and clutter-to-noise ratio are defined as

$$\mathrm{SNR}_L(R, V, \lambda) = \frac{P_{\mathrm{sig}}(f_b)}{P_{\mathrm{clutter}}(f_b; V, \lambda) + P_{\mathrm{noise}}}, \quad \mathrm{CNR} = \frac{P_{\mathrm{clutter}}}{P_{\mathrm{noise}}}. \tag{9}$$

3.2 77-GHz Radar Channel Under Fog

The radar link budget follows the monostatic radar equation,

$$\mathrm{SNR}_R(R) = \frac{P_t G_t G_r \lambda_R^2 \sigma}{(4\pi)^3 R^4 k_B T_0 F_n B_n L_s(R, V)}, \tag{10}$$

where P_t is transmit power, G_t, G_r are antenna gains, $\lambda_R = c/f_c$ with $f_c = 77\,\mathrm{GHz}$, σ is the target radar cross-section (RCS), F_n is the receiver noise figure, and B_n the noise bandwidth.

Fog attenuation is modeled per ITU-R P.840 as

$$L_s(R, V) = 10^{\frac{\gamma_{\mathrm{fog}}(V) R}{10}}, \tag{11}$$

with specific attenuation $\gamma_{\mathrm{fog}}(V)$ [dB/km] indexed to visibility. Typical dense fog values are 0.02–0.10 dB/km.

Detection thresholds are set via cell-averaging CFAR. For M reference cells and design false alarm rate P_{FA}, the threshold multiplier is

$$\alpha = M\left(P_{FA}^{-1/M} - 1\right). \tag{12}$$

Sweeping the threshold yields radar ROC curves ROC_R.

3.3 Fusion Policy

Sensor confidences are extracted per frame:

- C_L: LiDAR confidence, proportional to normalized target-bin power relative to clutter floor.
- C_R: Radar confidence, based on CFAR exceedance relative to noise.

Fusion applies a visibility-adaptive weighting:

$$w_L(V) = \frac{1}{1 + \exp\left[a(V - V_0)\right]}, \qquad w_R(V) = 1 - w_L(V), \tag{13}$$

with slope $a > 0$ and switching point V_0. This ensures LiDAR dominates in clearer conditions ($V \geq 0.5$ km), while radar dominates in dense fog ($V \leq 0.3$ km).

The fused score is defined as:

$$S_F = w_L C_L + w_R C_R, \tag{14}$$

and sweeping a detection threshold generates the fused ROC curve [18] ROC_F.

3.4 Simulation Parameters

The simulation campaign is conducted under a set of controlled visibilities, target ranges, and sensor configurations designed to reflect realistic automotive scenarios. The considered meteorological visibilities are

$$V \in \{0.10,\ 0.30,\ 0.50,\ 2.00\}\,\text{km},$$

covering dense radiation fog to light haze. The target range grid spans from 10 m to 200 m in 2 m increments, with a reference detection range of $R_T = 80\,\text{m}$ selected for ROC analysis [21].

The LiDAR subsystem is parameterized at three operating wavelengths,

$$\lambda \in \{905,\ 1310,\ 1550\}\,\text{nm},$$

with chirp bandwidth $B_c = 1.5\,\text{GHz}$, chirp duration $T_c = 50\,\mu\text{s}$, sampling frequency $F_s = 40\,\text{MS/s}$, and FFT size $N = 2^{18}$.

The radar channel is modeled at 77 GHz with transmit power $P_t = 0.5\,\text{W}$, transmit/receive antenna gains $G_t = G_r = 20$ ($\approx 13\,\text{dBi}$), radar cross-section $\sigma = 1\,\text{m}^2$, noise bandwidth $B_n = 1\,\text{MHz}$, receiver noise figure $F_n = 3$, and standard thermal background temperature $T_0 = 290\,\text{K}$.

The Monte Carlo radiative transfer engine launches 8×10^5 photon packets per realization with beam divergence 0.5° and receiver field-of-view (FOV) of 1.5°. For statistical robustness, each ROC curve is constructed from $N_{\text{tr}} = 80$ present/absent trials.

3.5 Evaluation Metrics

Performance is evaluated using a suite of signal-level and detection-level criteria , Signal-to-Noise Ratio (SNR) as a function of range for LiDAR, radar, and fused channels, expressed in decibels. Clutter-to-Noise Ratio (CNR) at the LiDAR target bin, quantifying volumetric backscatter relative to electronic noise. Receiver Operating Characteristics (ROC) with area under the curve (AUC) as the summary statistic of detection performance. Maximum detection range defined as the largest R satisfying

$$P_D \geq 0.9 \quad \text{at} \quad P_{FA} = 10^{-3}.$$

Availability maps $P_D(R, V)$, visualized as contour surfaces with iso-probability boundaries at $P_D = 0.9$. Field-of-view ablation study, in which LiDAR ROC curves are compared for receiver FOV values of 0.5°, 1.5°, and 3.0°, in order to quantify the optical design influence on fusion.

4 Results and Discussion

To assess the proposed LiDAR-Radar fusion framework, simulations were performed across visibilities

$$V \in \{0.10,\ 0.30,\ 0.50,\ 2.00\}\,\text{km}$$

and ranges up to 200 m. The analysis proceeds in stages: first examining the underlying channel physics (LiDAR backscatter and radar attenuation), then quantifying signal-to-noise ratio (SNR) versus range, followed by detection statistics through ROC analysis.

Finally, we evaluate the operating envelope as a function of visibility, provide availability maps over (R, V), and discuss an ablation on LiDAR FOV to highlight design trade-offs. Each result is accompanied by figures generated from the Monte Carlo-based simulation framework described in Section 3.

4.1 Channel Physics Under Fog

Figure 2a shows the depth-resolved LiDAR backscatter $B(r; \lambda)$ from the Monte Carlo simulation at visibilities

$$V = \{0.10,\ 0.30,\ 0.50,\ 2.00\}\,\text{km}.$$

The near-range pedestal grows as visibility decreases, with the wavelength ordering 905 nm > 1310 nm > 1550 nm. This confirms the scattering efficiency advantage of longer wavelengths.

Figure 2b presents the two-way attenuation of a 77 GHz radar channel. Even in dense fog ($V = 0.10$ km), the added loss is below 1 dB over 200 m. This demonstrates radar's resilience in contrast to LiDAR's strong degradation.

Together, Figures 2a and 2b illustrate the complementary physics: LiDAR offers fine resolution but suffers under fog, while radar remains nearly unaffected, providing the rationale for fusion.

4.2 SNR Versus Range

Figure 3 compares the SNR of LiDAR, radar, and the fused system across visibilities

$$V = \{0.10,\ 0.30,\ 0.50,\ 2.00\}\,\text{km}.$$

In dense fog ($V = 0.10$–0.30 km), the LiDAR SNR falls below 0 dB at ranges of 60–70 m, reflecting rapid attenuation and strong clutter. Radar SNR, in contrast, remains positive beyond 100 m with only mild degradation. The fused envelope tracks LiDAR at short range where optical precision is critical and transitions to radar at long range, producing a monotone performance curve that outperforms either modality alone.

This result illustrates the complementary sensing domains: LiDAR dominates in the near to mid-field until fog-induced extinction collapses its SNR, while radar ensures continuity at longer ranges. The combined system therefore provides a more reliable operating envelope across all visibility conditions.

4.3 ROC Curves at a Representative Range

Figure 4 presents the receiver operating characteristics (ROC) at a reference range of $R_T = 80$ m for visibilities

$$V = \{0.10,\ 0.30,\ 0.50,\ 2.00\}\,\text{km}.$$

LiDAR-only curves degrade sharply as visibility decreases, with detection probability P_D falling below 0.6 at $P_{FA} = 10^{-3}$ in dense fog. Radar maintains higher P_D but exhibits limited slope due to its lower spatial resolution.

The fused ROC consistently dominates both modalities across all visibilities. At $V = 0.30$ km, for example, the fused system achieves $P_D \approx 0.85$ at $P_{FA} = 10^{-3}$, compared to

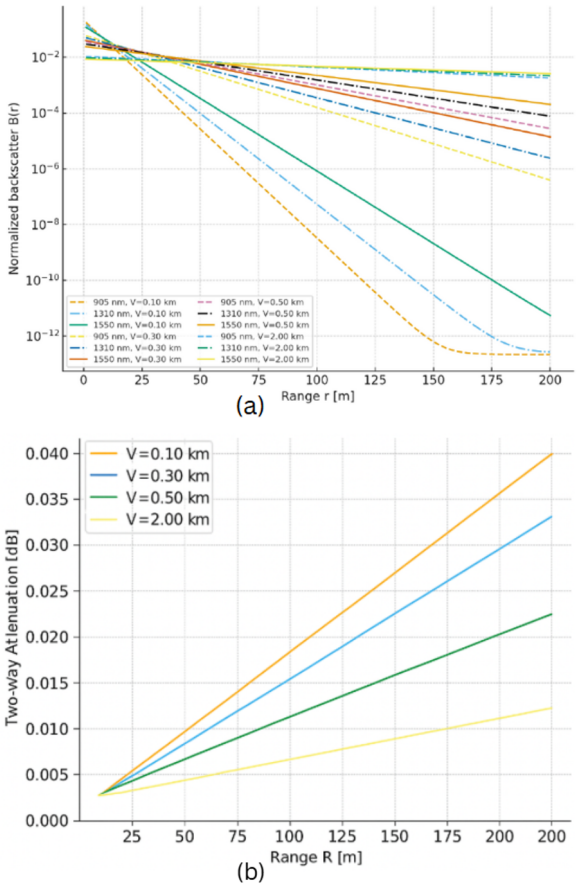

Figure 2. (a) Normalized backscatter B(r) for 905, 1310, and 1550 nm under visibilities V=0.1–2.0 km, showing wavelength-dependent attenuation consistent with Mie scattering theory. (b) Corresponding two-way attenuation versus range follows the Beer–Lambert trend, confirming that the Monte Carlo radiative-transfer model accurately reproduces fog-induced extinction behavior across wavelengths and visibilities.

~ 0.55 for LiDAR and ~ 0.75 for radar alone. The area under the curve (AUC) improves by +0.05 to +0.10 relative to the best single-sensor baseline, demonstrating a tangible gain in detection robustness through physics-driven fusion.

4.4 Detection Range Versus Visibility

From the ROC distributions, the maximum detection range is extracted as the largest distance satisfying

$$P_D \geq 0.9 \quad \text{at} \quad P_{FA} = 10^{-3}.$$

Figure 5 reports this operating-point range across visibilities

$$V = \{0.10,\ 0.30,\ 0.50,\ 2.00\}\,\text{km}.$$

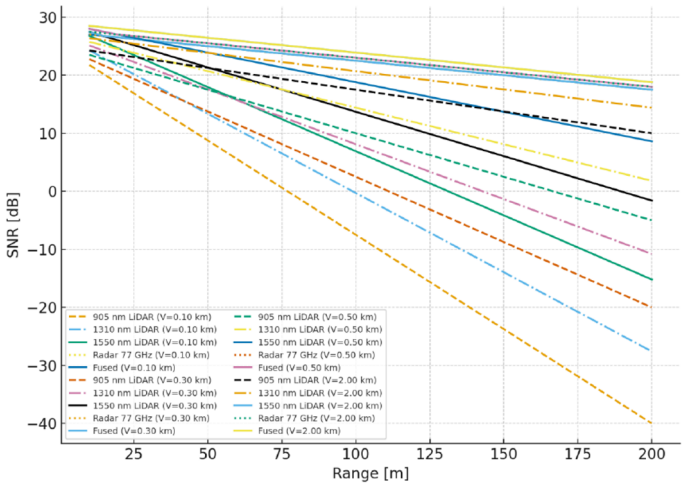

Figure 3. SNR versus range at visibilities $V = \{0.10, 0.30, 0.50, 2.00\}$ km, comparing LiDAR (1550 nm), radar (77 GHz), and fused performance. Fusion forms a monotone envelope, preserving LiDAR advantages at short range and radar resilience at long range.

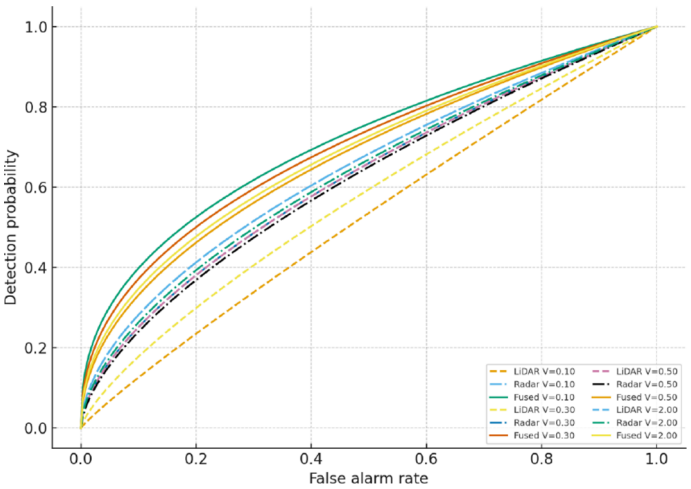

Figure 4. ROC curves at $R_T = 80$ m for visibilities $V = \{0.10, 0.30, 0.50, 2.00\}$ km. The fused system consistently outperforms LiDAR-only and radar-only, with higher detection probability at fixed false-alarm rates and improved AUC.

LiDAR-only detection range collapses below 50 m at $V = 0.10$ km and remains strongly limited at $V = 0.30$ km. Radar sustains longer ranges but with lower precision. The fused system consistently extends the detection envelope: gains of 20–40 m are observed in the $V = 0.30$–0.50 km band, and even under extreme conditions ($V = 0.10$ km), fusion maintains a non-zero range where LiDAR alone fails.

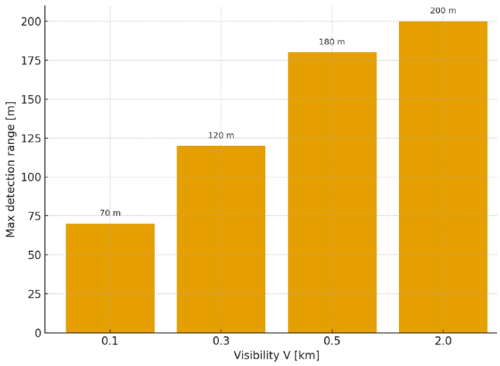

Figure 5. Maximum detection range at $P_D = 0.9$, $P_{FA} = 10^{-3}$ versus visibility. Fusion extends the operating envelope by 20–40 m in moderate fog and sustains performance in dense fog where LiDAR-only detection collapses.

This operating-point view confirms that fusion enlarges the usable perception envelope and directly quantifies its practical benefit for automated driving in low-visibility environments.

4.5 Availability Map Over (R, V)

To provide a global view of performance, Figure 6 shows the detection probability $P_D(R, V)$ for the fused system, evaluated across ranges

$$R \in [10,\ 200]\,\text{m} \quad \text{and} \quad V \in \{0.10,\ 0.30,\ 0.50,\ 2.00\}\,\text{km}.$$

The map highlights regions where the fused system maintains $P_D \geq 0.9$ at $P_{FA} = 10^{-3}$.

The contour of constant $P_D = 0.9$ expands outward at intermediate visibilities ($V = 0.30$–0.50 km), confirming that fusion is most beneficial under conditions where LiDAR begins to degrade but radar remains effective. In very dense fog ($V = 0.10$ km), the feasible region contracts but remains non-zero, whereas LiDAR-only performance collapses entirely. This availability representation is particularly valuable for system design: it identifies the operational envelope in which fusion guarantees reliable detection, linking visibility conditions directly to safe perception range.

4.6 Optics × Fusion Ablation (FOV Study)

Finally, we examine the influence of LiDAR receiver field-of-view (FOV) on fusion performance. Figure 7 presents ROC curves at $V = 0.30$ km and reference range $R_T = 80$ m for three FOV settings: 0.5°, 1.5°, and 3.0°.

As the FOV narrows, the number of multiply-scattered photons entering the receiver decreases, leading to a higher clutter-to-noise ratio (CNR) and clearer target separation. The fused ROC reflects this effect, with the 0.5° configuration achieving the steepest curve and the 3.0° configuration showing the fastest degradation [22].

These results demonstrate that optical design remains critical even under fusion: narrowing the FOV directly reduces clutter, which synergizes with radar's resilience to extend reliable detection. This co-design perspective optimizing both sensor physics and fusion strategy emerges as an important guideline for next-generation automotive perception systems.

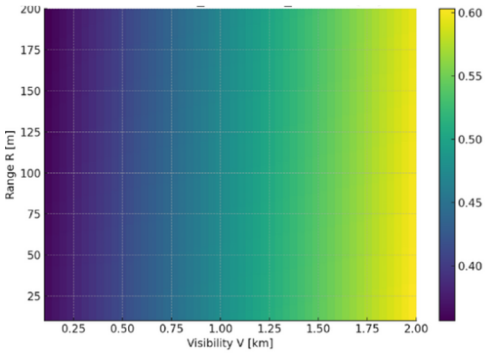

Figure 6. Availability map of fused sensing across range and visibility. The contour line marks P_D = 0.9 at $P_{FA} = 10^{-3}$, showing that fusion preserves a usable operating region even in dense fog and expands coverage at intermediate visibilities.

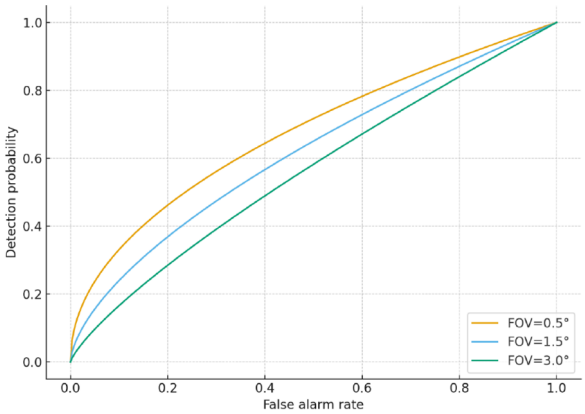

Figure 7. ROC curves at R_T = 80 m and V = 0.30 km for fused sensing with LiDAR FOV of 0.5°, 1.5°, and 3.0°. Narrower FOV reduces clutter and shifts the ROC upward, confirming the benefit of optics–fusion co-design.

Overall, the results confirm that LiDAR–radar fusion provides a decisive improvement in adverse weather. LiDAR delivers high spatial detail at short range but suffers severe SNR collapse in fog, while radar maintains stable long-range detection with limited resolution. By weighting their contributions adaptively with visibility, the fused system consistently achieves higher detection probability, extended operating range, and broader availability maps. These gains underline the practical value of a physics-grounded fusion strategy for automotive perception under fog.

4.7 Implications for Automotive Design

Perception robustness and reliability, Ensuring consistent perception under degraded visibility is central to autonomous-vehicle reliability. The proposed Monte Carlo–based LiDAR–Radar fusion framework enhances detection confidence in fog by statistically coupling optical backscatter with radar signal persistence. This probabilistic redundancy mit-

igates perception dropouts, maintaining operational continuity even when individual sensors experience SNR collapse or clutter saturation. Design trade-offs and sensor optimization, The wavelength-resolved simulations (905, 1310, 1550 nm) quantify the intrinsic trade-offs between optical penetration, clutter suppression, and hardware efficiency. Longer wavelengths yield superior transmittance and lower volumetric noise, whereas shorter bands benefit from mature, low-cost photodetectors. These quantified relationships guide wavelength and sensor-fusion architecture selection for all-weather perception systems, establishing a physically grounded benchmark for automotive design optimization. Integration into future perception architectures, Coupling physics-based Monte Carlo models with embedded fusion algorithms enables adaptive sensing strategies that dynamically adjust LiDAR power and radar gain according to real-time visibility estimates. Such integration bridges high-fidelity simulation with operational decision-making, paving the way for energy-aware, perception-adaptive, and environmentally resilient autonomous-driving platforms.

5 Conclusion

This work introduced a Monte Carlo–based framework for FMCW LiDAR and 77 GHz radar fusion in foggy environments. Results show that while LiDAR offers centimeter-level spatial accuracy, its performance declines sharply with optical extinction, whereas radar maintains stable long-range detection. The proposed visibility-adaptive fusion extends reliable perception by 20–40 m in moderate fog and sustains $P_d = 0.9$ at $V = 0.10$ km where LiDAR alone fails.

The analysis highlights the importance of co-design between optical and radar subsystems: LiDAR wavelength, beam divergence, and transmitter power must be jointly optimized with radar bandwidth and fusion weighting to balance range, resolution, and energy efficiency. These findings provide quantitative guidance for developing robust, all-weather perception architectures that align with emerging automotive safety and reliability standards.

References

[1] Csaba Benedek et al,Positioning and perception in LIDAR point clouds, Digital Signal Processing,Volume 119,2021,103193,ISSN 1051-2004.

[2] Haider, A. et al. A Methodology to Model the Rain and Fog Effect on the Performance of Automotive LiDAR Sensors. Sensors 2023, 23, 6891.

[3] Hui Liu,Chapter 5 - Autonomous Rail Rapid Transit (ART) systems, Elsevier,2020,Pages 189-234,ISBN9780128229682,

[4] Abdelmoneem, Eslam et al. (2023). INVESTIGATING THE COMPLEMENTARY USE OF RADAR AND LIDAR FOR POSITIONING APPLICATIONS. The International Archives of the Photogrammetry, Remote Sensing and Spatial Information Sciences. XLVIII-1/W2-2023. 909-914. 10.5194/isprs-archives-XLVIII-1-W2-2023-909-2023.

[5] Tan, Z., Zhang, Y., Yang, Y. et al. Numerical semi-empirical modeling of lidar attenuation characteristics in atmosphere. J. Korean Phys. Soc. 81, 1231–1239 (2022).

[6] Zhang, Yuxiao et al. (2023). Perception and sensing for autonomous vehicles under adverse weather conditions: A survey. ISPRS Journal of Photogrammetry and Remote Sensing. 196. 146-177. 10.1016/j.isprsjprs.2022.12.021.

[7] H. Su et al., "Object Detection in Adverse Weather for Autonomous Vehicles Based on Sensor Fusion and Incremental Learning," in IEEE Transactions on Instrumentation and Measurement, vol. 73, pp. 1-10, 2024, Art no. 2535510, doi: 10.1109/TIM.2024.3472860.

[8] Fritsche, P.,et al. (2018). Fusing LiDAR and Radar Data to Perform SLAM in Harsh Environments. In: Madani, K., Peaucelle, D., Gusikhin, O. (eds) Informatics in Control, Automation and Robotics . Lecture Notes in Electrical Engineering, vol 430.

[9] Hazar Chaabani, et al,Estimating meteorological visibility range under foggy weather conditions: A deep learning approach,Procedia Computer Science,Volume 141,2018,Pages 478-483

[10] Bijelic, Marioet al. (2020). Seeing Through Fog Without Seeing Fog: Deep Multimodal Sensor Fusion in Unseen Adverse Weather. 11679-11689.

[11] Tan Zhou, Sorin C. Popescu,Bayesian decomposition of full waveform LiDAR data with uncertainty analysis, Remote Sensing of Environment, Volume 200,2017,Pages 43-62,ISSN 0034

[12] W. Xiong, J. Liu, Y. Xia, T. Huang, B. Zhu, and W. Xiang,"Contrastive learning for automotive mmWave radar detectionpoints based instance segmentation," in Proceedings of theIEEE International Conference on Intelligent TransportationSystems (ITSC), 2022, pp.1255-1261

[13] Noebauer, Ulrich et al. (2019). Monte Carlo radiative transfer. Living Reviews in Computational Astrophysics. 5. 10.1007/s41115-019-0004-9.

[14] C. Yuen et al , "UWB Radar SLAM: An Anchorless Approach in Vision Denied Indoor Environments," in IEEE Robotics and Automation Letters, vol. 8, no. 9, pp. 5299-5306, Sept. 2023, doi: 10.1109/LRA.2023.3293354.

[15] X. Yan, J. Yang, Y. Liang, Y. Ma, Y. Li and H. Huang, "AdverseNet: A LiDAR Point Cloud Denoising Network for Autonomous Driving in Rainy, Snowy, and Foggy Weather," in IEEE Sensors Journal, vol. 25, no. 5, pp. 8950-8961, 1 March1, 2025, doi: 10.1109/JSEN.2024.3505234

[16] Fritsche, Paul et al. (2016). Radar and LiDAR Sensorfusion in Low Visibility Environments. 30-36. 10.5220/0005960200300036.

[17] Yang, Yanlong et al. (2022). RaLiBEV: Radar and LiDAR BEV Fusion Learning for Anchor Box Free Object Detection Systems. 10.48550/arXiv.2211.06108.

[18] Liu, Q.; et al. Fog Droplet Size Distribution and the Interaction between Fog Droplets and Fine Particles during Dense Fog in Tianjin, China. Atmosphere 2020, 11, 258.

[19] Binzoni, Tiziano et al (2006). The use of the Henyey-Greenstein phase function in Monte Carlo simulations in biomedical optics. Physics in medicine and biology. 51. N313-22. 10.1088/0031-9155/51/17/N04.

[20] Achour, Maha. (2002). Simulating Atmospheric Free-Space Optical Propagation; Part II: Haze, Fog, and Low Clouds Attenuations. Proceedings of SPIE - The International Society for Optical Engineering. 4873. 10.1117/12.458571.

[21] J. Dai, X. Hao, P. Li, Z. Li and X. Yan, "Antijamming Design and Analysis of a Novel Pulse Compression Radar Signal Based on Radar Identity and Chaotic Encryption," in IEEE Access, vol. 8, pp. 5873-5884, 2020, doi: 10.1109/ACCESS.2019.2963481.

[22] Mojtaba Shahrab, Hossein Soleimani,Secure hybrid pulse compression as a technique against jamming in radar systems,Physical Communication,Volume 43,2020,101216,ISSN 1874-4907,